HHS Public Access

Author manuscript

Cell Rep. Author manuscript; available in PMC 2018 November 20.

Published in final edited form as:

Cell Rep. 2018 October 23; 25(4): 1040–1050.e5. doi:10.1016/j.celrep.2018.09.081.

Jumonji Inhibitors Overcome Radioresistance in Cancer through Changes in H3K4 Methylation at Double-Strand Breaks

Juan Bayo[1,3], **Tram Anh Tran**[#2], **Lei Wang**[#2], **Samuel Peña-Llopis**[4], **Amit K. Das**[#2], and **Elisabeth D. Martinez**[1,2,6,*]

[1]Department of Pharmacology, UT Southwestern Medical Center, Dallas, TX, USA

[2]Hamon Center for Therapeutic Oncology Research, UT Southwestern Medical Center, Dallas, TX, USA

[3]Instituto de Investigaciones en Medicina Traslacional, CONICET, Universidad Austral, Argentina

[4]Division of Translational Oncology, Essen University Hospital, German Cancer Consortium (DKTK), Partner Site Essen and German CancerResearch Center (DKFZ), Heidelberg, Germany

[6]Lead Contact

[#] These authors contributed equally to this work.

SUMMARY

We have uncovered a role for Jumonji inhibitors in overcoming radioresistance through KDM5B inhibition. Pharmacological blockade of Jumonji demethy-lases with JIB-04 leads to specific accumulation of H3K4me3 at sites marked by γH2AX and impaired recruitment of DNA repair factors, preventing resolution of damage and resulting in robust sensitization to radiation therapy. In DNA-repair-proficient cancer cells, knockdown of the H3K4me3 demethylase KDM5B, but not other Jumonji enzymes, mimics pharmacological inhibition, and KDM5B overexpression rescues this phenotype and increases radioresistance. The H3K4me3 demethylase inhibitor PBIT also sensitizes cancer cells to radiation, while an H3K27me3 demethylase inhibitor does not. *In vivo* co-administration of radiation with JIB-04 significantly prolongs the survival of mice with tumors even long after cessation of treatment. In human patients, lung squamous cell carcinomas highly ex-pressing KDM5B respond poorly to radiation. Thus, we propose the use of Jumonji KDM inhibitors as potent radiosensitizers.

In Brief

[*]Correspondence: elisabeth.martinez@utsouthwestern.edu.

AUTHOR CONTRIBUTIONS

J.B. performed experiments, analyzed data, and helped write the manuscript; T.A.T., L.W., and A.K.D. performed experiments, analyzed data, and aided in figure preparation; S.P.-L. analyzed human sample data; and E.D.M. guided the work, analyzed data, and wrote the manuscript.

DECLARATION OF INTERESTS

The authors declare no competing interests.

SUPPLEMENTAL INFORMATION

Supplemental Information includes eight figures and six tables and can be found with this article online at https://doi.org/10.1016/j.celrep.2018.09.081.

Radioresistance is an obstacle to lung cancer cures. Bayo et al. reveal that JARID1B removes H3K4me3 marks at sites of DNA damage. Genetic or pharmacological inhibition of JARID1B robustly radiosensitizes cancers in vitro and *in vivo* through defects in DNA repair, providing a therapeutic option for radioresistant tumors.

Graphical Abstract

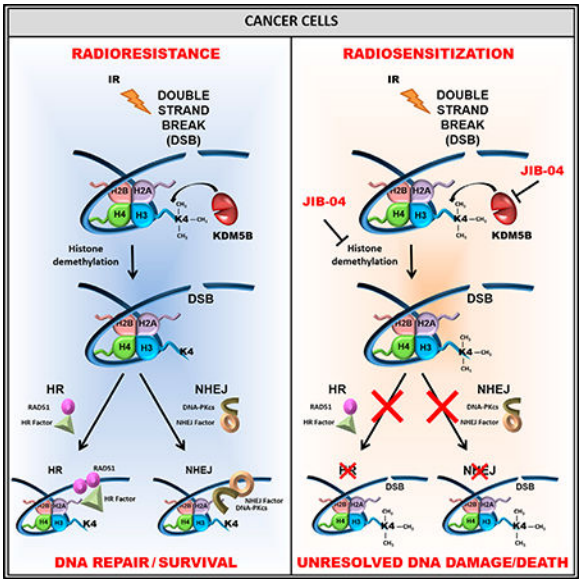

INTRODUCTION

Toxicity from and resistance to radiation therapy constitutes a major obstacle to curative treatments for non-small cell lung cancer (NSCLC) and other solid malignancies. Current regimens for radiation therapy employ radiation alone or concurrent with cycles of standard chemotherapy (Das et al., 2010; Song et al., 2014). This is often limited by toxicity to normal tissues and is complicated by the development of resistance (Anscher, 2010; Crinó et al., 2010; Eberhardt et al., 2006; Falkson et al., 2017; Howington et al., 2013). Although the use of targeted therapies to radiosensitize is not yet current practice, DNA repair inhibitors, for example, have been tested in preclinical models and show efficacy (Gil del Alcazar et al., 2014, 2016; Provencio and Sa´ nchez, 2014; Tofilon and Camphausen, 2009).

Ionizing radiation (IR) results in a wide variety of chromosomal DNA damage, with double-strand DNA breaks (DSBs) being the main lesion involved in mitotic failure and cell death (Ward, 1988). As a response to DSBs, a highly regulated signaling pathway is activated to initiate repair mechanisms including homologous recombination (HR) or non-homologous end joining (NHEJ), de-pending on cell-cycle phase and cellular state (Chapman et al., 2012; Jeggo et al., 2011). One of the earliest events in this cascade is the phosphorylation by the serine/threonine kinase ataxia telangiectasia mutated (ATM) of a histone variant, H2AX, which marks sites of damage and triggers the recruitment of the repair machinery (Firsanov et al., 2011; Karagiannis and ElOsta, 2007; Kinner et al., 2008). 53BP1 is subsequently recruited, and its Tudor domain is thought to function in reading the methylation state of the

chromatin at damage sites (Mallette et al., 2012). Other histone modifiers, especially methylation readers and erasers, directly or indirectly also mediate aspects of DSB repair (Fnu et al., 2011; Hunt et al., 2013; Watanabe et al., 2013). In active euchromatic regions, for instance, it has been reported that transcription is halted upon DNA damage, and this is mediated at least in part by the recruitment of repressive complexes, including PRC1, and by ubiquitination of H2A (Ui et al., 2015; Wu et al., 2013). Heterochromatin regions marked by H3K9me3 are more refractory to DSB repair (Goodarzi et al., 2008; Janssen et al., 2016; Tsouroula et al., 2016), and thus, for example, the Jumonji histone demethylases KDM4B and KDM4D appear to be recruited to DSB sites early on to reduce H3K9me3/H3K9me2 local levels (Young et al., 2013). A further example is given by a recent report that uncovered a role of JMJD5 or KDM8 in the late stages of HR via regulation of H3K36me2 marks (Amendola et al., 2017).

We have identified and characterized an inhibitor of Jumonji enzymes, JIB-04, that selectively targets lung cancer cells versus normal cells (Bayo et al., 2015; Dalvi et al., 2017; Wang et al., 2013). In the present study, we demonstrate that JIB-04 and inhibitors of H3K4me3 demethylases, but not of H3K27me3 demethylases, sensitize radioresistant NSCLC to radiation, impairing both NHEJ and HR. JIB-04 causes the retention of H3K4me3 marks near DSBs and impairs recruitment of repair factors. Overexpression of the H3K4me3 demethylase KDM5B, a target of JIB-04 inhibition, rescues the DNA repair defects induced by JIB-04. Increasing the levels of KDM5B also abolishes the radiosensitization action of JIB-04 and promotes radiation resistance. *In vivo*, Jumonji inhibition robustly enhances the effects of radiation treatment and prolongs survival. Analysis of cancer patient data uncovered a correlation between high expression of KDM5B and radiation resistance in human lung tumors. This work suggests that KDM5B plays an essential role in the repair of DSB at transcriptionally active loci and has implications for the treatment of radiation resistant cancers and for achieving enhanced response to radiation therapy in patients. Thus, we provide proof-of-principle studies in support of the use of Jumonji or KDM5 inhibitors to overcome radiation resistance.

RESULTS

Inhibitionof Jumonji Enzymes withJIB-04 Enhances the Response of Cancer Cells to Radiation

We first evaluated whether inhibition of Jumonji histone demethylases, which should increase histone methylation, would alter the response to radiation due to the underlying known connections between histone methylation and DNA repair. To this end, we treated radioresistant NSCLC lines H1299 or A549 with our pan-selective Jumonji inhibitor JIB-04 (Dalvi et al., 2017; Martinez and Gazdar, 2016; Wang et al., 2013) or vehicle, and then exposed the cells to increasing levels of IR. Colony-formation IC_{50} doses of JIB-04 were calculated to be in the nano-molar range (Figure S1A) and were used in combination with radiotherapy in standard colony-formation assays. Treatment with JIB-04 4 hr prior to IR exposure robustly increased the intrinsic radiosensitivity of these radioresistant cell lines (Figures 1A and 1B) and markedly decreased the surviving fraction at 2 Gy radiation (SF2) (Table S1). Only the active E-isomer of JIB-04 had this radiosensitizing effect, which was

not observed with the inactive Z-isomer (Wang et al., 2013). Sensitization to radiation and decreased SF2 were also seen for multiple other strongly or moderately radioresistant NSCLC lines tested, as well as for other tumor types (Table S1; Figures S1B and S1C). These changes in SF2 values are more robust than what has been reported, such as for PARP1 inhibitors in various cancer types (Lesueur et al., 2017). Interestingly, the dose enhancement ratio at 25% cell kill, DER25 (the radiation dose required to reduce the survival fraction to 25% in the absence or presence of JIB-04) was higher for cells that were more radioresistant and consequently had high SF2 values than for cells with intrinsically lower SF2 values (Table S1). Additionally, the radiosensitization caused by JIB-04, as measured by decreasing SF2 values, was dose dependent (Figures 1C and 1D).

To evaluate the optimal timing of Jumonji inhibition for enhancing the response to radiation, we compared the effects of administering JIB-04 prior to versus after IR in NSCLC lines (Figure S1D). Sensitization was observed under both conditions but was significantly more robust when administering JIB-04 4 hr prior to IR (Figure S1E). Thus, the radiosensitization action of JIB-04 is most effective before DNA repair begins in response to radiation damage. Taken together, these data suggest the Jumonji inhibitor may act upstream of or impact DNA repair.

γH2AX and 53BP1 Foci Resolution after IR Is Delayed by JIB-04, but Not GSK-J4, Treatment

To determine whether JIB-04 radiosensitizes cells by affecting DNA repair, repair-proficient NSCLC cells (H1299 and A549) were pretreated for 4 hr with colony-formation IC_{50} doses of this pan-Jumonji inhibitor (Figure S1A) and then exposed to IR in the continuous presence of the drug. In JIB-04-treated cells, ATM signaling was activated in response to IR similar to the vehicle control (Figure S2A) and calculated to be in theH2AX foci formation was also intact (Figures 2A and 2B, 15 min, red channel). However, the time-dependent decrease in γH2AX foci corresponding to damage resolution was significantly impaired in the presence of JIB-04 (Figures 2A and 2B, red channel and upper bar graphs) with >30% of foci remaining unresolved even at late time points. Similarly, 53BP1 foci resolution was defective in cells treated with IR plus JIB-04 compared to IR alone, and foci accumulation re-mained (Figures 2A and 2B, green channel and lower bar graph). The same was true in other radioresistant NSCLC lines (Table S2). Importantly, JIB-04 on its own did not cause DNA damage (Figure S2B). JIB-04 also prevented resolution of DNA damage in prostate cancer LNCaP cells (Figure S2C). Furthermore, the defects in DNA repair dynamics induced by JIB-04 were not the result of altered distribution of cells through the cell cycle or of preventing the signature G2/M arrest caused by IR (Figures S3A and S3B).

We then evaluated the effects of another Jumonji inhibitor, GSK-J4, on the DNA repair process. In contrast to the pan-inhibition of Jumonji enzymes seen with JIB-04 (Dalvi et al., 2017; Wang et al., 2013), GSK-J4 has been reported to more specifically target Jumonji H3K27 demethylases at low or moderate doses (Kruidenier et al., 2012). We have previously confirmed that in NSCLC cells, including H1299, GSK-J4 only affects H3K27me3 demethylation and not H3K4me3 or H3K9me3 de-methylation and that this specificity is maintained *in vivo* (Dalvi et al., 2017; see Figure 6F in Dalvi et al., 2017). Here, we first

established GSK-J4's potency against H1299 and A549 NSCLCs in colony-formation assays (Figure S3C) and then exposed cells to IC_{50} doses in the presence of radiation, as done with JIB-04. In contrast to JIB-04, however, GSK-J4 failed to sensitize radioresistant NSCLC cells (Figure S3D). Consistent with this result, GSK-J4 had no impact on the resolution of IR-induced damage as measured by γH2AX or 53BP1 foci resolution in H1299 (Figure S4A) or A549 cells (Figure S4B). This indicated that targets specific to JIB-04, but not GSK-J4, under the tested conditions (likely H3K4me3 and/or H3K9me3 demethylases) (see Dalvi et al., 2017, Figures 6F and 6G) play a role in DNA repair dynamics and radiation sensitivity in NSCLC.

Inhibition of Jumonji Enzymes Does Not Radiosensitize or Affect the DNA Repair Dynamics of Normal Cells

We have previously established that JIB-04 specifically inhibits the viability of cancer cells, but not normal cells, and selectively alters cancer cell transcription (Dalvi et al., 2017; Wang et al., 2013). To determine whether the effect of JIB-04 on DNA repair dynamics described above was also cancer-selective, we evaluated the response to radiation of two different normal human bronchial epithelial cell (HBEC) lines derived from two distinct patients and immortalized for culture, HBEC3KT and HBEC30KT, which remain non-tumorigenic (Sato et al., 2006, 2013). IC_{50} doses of JIB-04 in colony-formation assays (Figure 3A) were used to pretreat cells 4 hr prior to radiation, and then survival was measured as before. Remarkably, JIB-04 did not radiosensitize these normal cells (Figure 3B). In agreement with these findings, in normal cells treated with inhibitor, no defects were found in γH2AX foci formation in response to IR in foci resolution over a time course (Figure 3C), or in DNA damage signaling (Figure S3E). These data indicate that the DNA repair deficiency and consequent radiosensitization triggered by JIB-04 are cancer specific.

JIB-04 Lowers the Efficiency of Both NHEJ and HR

To understand the mechanism for the delayed resolution of IR-induced damage seen in cancer cells in the presence of JIB-04, we measured the efficiency of repair by NHEJ and HR, the two main pathways of cellular DSB repair. Established plasmid-based reporter systems were used for this purpose (Seluanov et al., 2010). H1299 cells containing the stably integrated NHEJ or HR constructs depicted in Figure 4A were transfected with an I-Sce1 expression vector to induce DNA breaks and with an mCherry plasmid to control for transfection efficiency. Transfected cells treated with JIB-04 or vehicle were then assayed by fluorescence-activated cell sorting (FACS) for GFP expression as a measure of repair. As demonstrated in Figures 4B and S5A, both NHEJ and HR were significantly inhibited in the presence of JIB-04 to 50% or less of normal levels. These results were confirmed in other tumor types, which gave highly similar results (Figures S5B–S5D). In addition, NSCLC cells endogenously deficient in DNA repair and thus highly sensitive to IR were not further sensitized by JIB-04 (Figure S5E). Taken together, these findings point to a common upstream defect in the repair of DSBs caused by JIB-04, affecting both NHEJ and HR and leading to radiosensitization in DNA-repair-proficient cells. Thus, we next measured the recruitment of repair factors to sites of damage.

JIB-04 Blocks the Recruitment of DNA-PKcs and RAD51 to Sites of Damage and Inhibits Foci Resolution

The DNA-dependent protein kinase DNA-PKcs acts at sites of damage to mediate repair by NHEJ. Since we observed decreased efficiency of DNA repair by NHEJ after IR in cells treated with JIB-04, we measured the dynamics of active DNAPKcs foci formation and resolution. H1299 cells treated with IR readily formed DNA-PKcs pT2609 foci by 1 hr, and these foci were largely resolved by 24 hr (Figures 4C and 4D, white bars). In contrast, cells treated with JIB-04 plus IR exhibited a clear deficiency in forming active DNA-PKcs foci with delayed foci formation post-IR. In addition, the majority of DNA-PKcs pT2609 foci remained unresolved even 24 hr post-irradiation in the presence of the inhibitor (Figures 4C and 4D, black bars). Thus, JIB-04 both impaired the timely recruitment of active DNA-PKcs to sites of damage and blocked their resolution.

To determine whether JIB-04 was also impairing proper recruitment of HR factors to sites of damage, we measured RAD51 foci formation and resolution over a time course. Accumulation of RAD51 near DSBs was not seen at 3 hr but was readily detected by 6 hr in H1299 cells, consistent with the slower timing of HR compared to NHEJ (Figures 4E and 4F, white bars). JIB-04 treatment significantly diminished RAD51 recruitment and additionally impaired foci resolution, with a large percentage of foci remaining at late time points (Figures 4E and 4F, black bars). A similar behavior was observed in A549 cells (Figure S5F). Collectively, these data confirm that JIB-04 affects an aspect of DSB repair common to both NHEJ and HR.

Jumonji Inhibition by JIB-04 Results in H3K4me3, but Not H3K9me3, Enrichment at DSBs

Heterochromatin marked by H3K9me3 is more refractory to DNA repair than euchromatin (Chiolo et al., 2013). In euchromatin, H3K4me3 at transcriptionally active genes must likely be demethylated upon DNA damage in order to stop transcription until the DNA is repaired (Aymard et al., 2014; Iacovoni et al., 2010; Seiler et al., 2011; Solovjeva et al., 2007; Ui et al., 2015). Since inhibition of Jumonji histone demethylase enzymes with JIB-04 can result in increased histone methylation levels, we hypothesized that H3K4me3 or H3K9me3 marks may be accumulating around DSBs in drug-treated cells, contributing to defective repair factor recruitment and defective resolution of damage. To test this possibility, we immunoprecipitated global DNA fragments digested to single nucleosome size associated with γH2AX and then measured H3K4me3 or H3K9me3 levels at these sites of damage in cells treated with IR alone or with IR plus JIB-04 or DMSO vehicle. Surprisingly, there were no changes in H3K9me3 levels induced by JIB-04 at nucleosomes marked by γH2AX (Figures 5A and 5B, right panels). However, JIB-04 markedly increased H3K4me3 at these sites (Figures 5A and 5B, left panels). Consistent with this result, we found that the total enzy-matic activity of H3K4me3 Jumonji demethylasess (Figure 5C),but not that of H3K9me3 demethylases (Figure 5D), could be increased upon IR exposure and that just 4 hr of pretreatment with JIB-04 blocked this IR-induced increase in enzyme activity (Figures 5C and 5D). Under these experimental conditions, we again observed accumulation of γH2AX but no measurable changes in global histone marks (Figures S6A–S6C). While JIB04 treatment resulted in H3K4me3 accumulation at γH2AX-positive nucleosomes (Figures 5A and 5B, left panels), we did not see significant defects in Ku70 recruitment or protein levels

after inhibition in NSCLC (Figures S6D and S6E), in contrast to the defects seen in DNA-PKcs and RAD51 above. To confirm that H3K4me3 levels were accumulating at DSBs, we performed chromatin immunoprecipitation (ChIP)/re-precipitation (re-ChIP) experiments in H1299 cells harboring an engineered I-Sce1 cut site. Chromatin immunoprecipitation of DNA associated with γH2AX followed by re-ChIP with H3K4me3 antibodies revealed enrichment of DNA fragments at and adjacent to the site of DSB in JIB-04 treated cells, as revealed by qPCR (Figure 5E). This enrichment was not seen in a control genomic region (Figure 5E). Together, these results indicate that an H3K4me3 Jumonji demethylase enzyme(s) may be inhibited by JIB-04 during the response to IR, leading to the specific accumulation of its trimethylated histone substrate at transcriptionally active regions harboring DNA damage.

Jumonji KDM Enzyme Knockdown Phenocopies the JIB-04 Repair Defect, and Overexpression of KDM5B Rescues It

To directly address whether JIB-04 was targeting a specific Jumonji demethylase after IR, we evaluated whether genetic downregulation of Jumonji demethylases would phenocopy the effects of JIB-04, resulting in defects in DSB repair. Knockdown of KDM5B or KDM4B, but not of other H3K4me3 or H3K9me3 Jumonji demethylases screened, resulted in accumulation of unresolved γH2AX and 53BP foci (Figures S7A–S7D, 6A, and 6B). To define which of these enzymes might be the target of JIB-04 in NSCLC leading to the drug-induced defect in DSB repair, we performed rescue experiments. KDM5B, but not KDM4B, overexpression rescued the JIB-04-induced accumulation of unresolved γH2AX and 53BP foci (Figures 6C, 6D, S7E, and S7F). The accumulation of unresolved DSBs seen in KDM4B knockdown NSCLC cells (Figures 6A and 6B) is likely due to further DNA damage, as has been reported to occur in other cancer cell types upon KDM4B depletion (Chen et al., 2014; Young et al., 2013; Zheng et al., 2014). Thus, among H3K4me3 and H3K9me3 demethylases, KDM5B plays an important role in the DNA damage response, and its genetic or pharmacological inhibition triggers a defect in DSB repair that can be exploited therapeutically to enhance radiation sensitivity. This is in line with the higher sensitivity to JIB-04 of KDM5/JARID enzymes compared to other Jumonji demethylases that we have observed in vitro (Wang et al., 2013). In further support of this conclusion, the KDM5 inhibitor PBIT (Sayegh et al., 2013) also ra-diosensitized multiple NSCLCs (Figures S7G and S7H) similar to JIB-04 and in contrast to the lack of effect of GSK-J4 (Figure S4). We used PBIT for this study because of its higher potency in our system compared to the other available KDM5 inhibitor, CPI-455 (Vinogradova et al., 2016), as seen in Figures S7G and S7H. These results are in agreement with the reported recruitment of KDM5B to sites of DSBs seen in another system (Li et al., 2014) and indicate a role for demethylation of H3K4me3 at tran-scriptionally active loci harboring DNA damage in NSCLCs.

To gain further mechanistic insights into the role of KDM5B in DSB repair and the enhanced response to IR in the presence of JIB-04, we overexpressed KDM5B in NSCLCs competent for DNA repair and measured their survival to IR with or without JIB-04. Remarkably, in line with the rescue of JIB-04-induced γH2AX and 53BP1 foci accumulation (Figures 6C and 6D), KDM5B overexpression also rescued the survival of JIB-04treated cells exposed to IR compared to control cells (Figure 6E). Furthermore,

KDM5B overexpression blocked JIB-04-mediated radiosensitization and decrease in demethylase activity, while control cells retained sensitivity and demethylase inhibition, confirming KDM5B is the main cellular target of JIB-04 yielding the radiosensitization phenotype (Figures 6F and S7I–S7J).

JIB-04 Blocks H3K4me3 Demethylation *In vivo*, Radiosensitizes Tumors, and Prolongs the Survival of Tumor-Bearing Mice

To determine whether Jumonji inhibition results in radiosensitization and tumor regression *in vivo*, we generated subcutaneous tumors of H1299 cells. Tumors were established to a volume of 200 mm^3 before initiating treatment with JIB-04, IR, or JIB-04 plus IR as described in detail in STAR Methods. JIB-04 was used as the inhibitor of choice because of its known activity in mice (Dalvi et al., 2017; Wang et al., 2013) compared to other KDM5 inhibitors. Treatment of tumor-bearing mice with the combination of JIB-04 plus IR gave robust synergistic inhibition of tumor growth compared to either treatment alone (Figure 7A, left panel). Indeed, tumors treated with the combined therapy grew significantly slower than those treated with vehicle or either single agent. This was seen, for example, by a large dose enhancement factor of 6.5 for time to reach a volume of 500 mm^3. Whereas it took 5–8 days on average for tumors treated with vehicle, JIB-04 alone, or IR to reach this volume, tumors in animals receiving JIB-04 with IR took 22 days to reach this size.

We also evaluated whether the radiosensitizing effects of JIB04 translated into longer survival of tumor-bearing animals after treatment. As can be seen in Figure 7A (right panel), mice treated with JIB-04 and IR survived significantly longer than mice treated with either agent alone or vehicle. This was a sustained effect, maintained even weeks after the end of treatment, giving the animals a median survival of 55 days compared to 14 days in the vehicle-treated cohort, 16 days with JIB-04 alone, or 36 days in the IR group. Thus, there was strong synergy between JIB04 and IR *in vivo* as shown by both robust reduction in tumor growth rate and increased median survival, even after cessation of treatment. Strong synergy between JIB-04 and IR *in vivo* and robust increase in survival was also seen in A549 xenograft tumors (Figure 7B), fully confirming these results in a second model. Furthermore, lysates of tumors harvested from each treatment group at the time of sacrifice showed a significant increase in H3K4me3 demethylase activity after IR and an inhibition of this increase by JIB-04 (Figures 7C and 7D), consistent with our earlier observations in cells (Figure 5C), suggesting that the KDM5B pathway is also relevant *in vivo*. No overt toxicities were observed in the combination treatments (Figure S8). Finally, we queried lung cancer The Cancer Genome Atlas (TCGA) data to determine whether levels of KDM5B correlate with the clinical response to radiation therapy in human patients. We found that high levels of KDM5B correlate with radioresistance among patients with lung squamous cell carcinomas, while no significant correlation was seen with the other members of the KDM5 or KDM4 subfamilies (Table S3).

DISCUSSION

Jumonji enzymes have been reported to play roles in DNA repair pathways. It has been suggested, for example, that chromatin dissociation of the H3K36me2 demethylase KDM2A

in response to ATM phosphorylation is critical for the NHEJ process (Cao et al., 2016; Fnu et al., 2011). Likewise, KDM4A degradation is required at sites of DNA damage, since it competes with 53BP1 for binding to H4K20me through its Tudor domain (Mallette et al., 2012). In this study, we have uncovered a role for KDM5B in demethylation of H3K4me3 at and near sites of DNA damage and an IR-induced increase in H3K4me3 demethylase activity in lung cancer cells and in tumors *in vivo*. We show that the catalytic activity of KDM5B is required to mediate full and efficient repair of DSBs. Importantly, we have identified a pharmacological preclinical strategy to impair this activity *in vivo* leading to radiosensitization of tumors by the Jumonji inhibitor JIB-04. Mechanistically, inhibition of KDM5B activity results in defective recruitment of repair factors, lower efficacy of repair by both HR and NHEJ, and consequently radiosensitization of lung cancer cells and tumors. Knockdown of KDM5B, in turn, phenocopies the effects of pharmacological inhibition of this enzyme on DNA repair, consistent with the radiosensitizing effects of silencing KDM5B in oral carcinomas (Lin et al., 2015). Overexpression of KDM5B reverts both the DNA repair defects and the radiosensitization induced by JIB-04 treatment, indicating KDM5B is the main target of JIB-04 inhibition under conditions of IR damage in DNA-repair-proficient cells. Other actions of JIB-04 in addition to KDM5B inhibition may possibly further enhance the radiosensitization phenotype.

Our overall findings are in agreement with the reported importance of KDM5B in maintaining genome stability (Li et al., 2014) and support the idea that H3K4me3 demethylation and partial chromatin condensation may be required for efficient recruitment of repair factors at active chromatin (Burgess et al., 2014; Li et al., 2014; Seiler et al., 2011). The enhanced response to radiation triggered by inhibition of KDM5B activity appears to be the result of inefficient DNA repair. Upon Jumonji inhibition, repair factor recruitment and resolution of DSB are defective due to the accumulation of H3K4me3 marks at transcriptionally active regions harboring damage. Specifically, we observe delayed phospho-DNA-PKcs and RAD51 recruitment and defects in resolution under conditions that accumulate H3K4me3 near DSB, in conceptual agreement with the reported defect in Ku70 and BRCA1 binding at DBS after KDM5B knockout in osteosarcoma cells (Li et al., 2014). In NSCLCs, however, we do not observe measurable changes in Ku70 at sites of DSBs induced by IR. Based on this, we propose that the DNA damage response superactivates KDM5B to demethylate H3K4me3 at transcriptionally active genomic regions harboring DNA DSBs. This action of KDM5B would halter transcription at these open chromatin sites until repair is finalized, consistent with the suggestion that there is active demethylation of H3K4me3 at sites of DSB (Seiler et al., 2011). This model complements the existing view that ATM activation leads to the phosphorylation of the ENL transcriptional elongation factor, the recruitment of the PRC1 complex, and the ubiquitination of H2A at transcriptionally active sites harboring DNA damage to silence transcription (Ui et al., 2015). Our data suggest that in addition, the active demethylation of H3K4me3 at these sites by KDM5B is a likely necessary parallel step that allows the haltering of transcription and efficient repair factor binding at and near DSB (Li et al., 2014).

The engagement of KDM5B in the cellular response to DSBs induced by IR defines a therapeutic opportunity. As we show here, pharmacological inhibition of its demethylase activity with JIB-04 or PBIT results in tumor cell radiosensitization. The *in vivo* synergy we

observe between IR and JIB-04 treatment, together with the robust extension of lifespan and increased survival even weeks post treatment, points to a clear clinical potential for this type of approach. Our finding that lung cancer patients whose squamous cell tumors express high levels of KDM5B are more refractory to radiation therapy highlights the clinical relevance of our observations. Our study suggests this radioresistance may be overcome by pharmacological inhibition of KDM5 enzyme activity, establishing a paradigm where histone methylation at DSBs can be safely targeted to modulate the response to IR.

STAR★METHODS

KEY RESOURCES TABLE

REAGENT or RESOURCE	SOURCE	IDENTIFIER
Antibodies		
Anti–phospho-Histone γH2AX (Ser139)	Millipore	Cat#05–636; RRID: AB_309864
Anti–tri-methyl-histone H3K9	Millipore	Cat#07-442; RRID: AB_310620
Anti-tri-methyl-histone H3K4	Millipore	Cat#07-473; RRID: AB_1977252
Anti-53BP1	Cell Signaling Technology	Cat#4937; RRID: AB_106954558
Anti-KDM5B	Cell Signaling Technology	Cat#3273; RRID: AB_1264191
Anti-KDM4B	Cell Signaling Technology	Cat#D7E6; RRID: AB_11140642
Anti-mouse IgG-HRP linked	Cell Signaling Technology	Cat#7076; RRID: AB_330924
Anti–Rad51	Abcam	Cat#ab-213; RRID: AB_302856
Anti-DNA-PKcs p-T2609	Abcam	Cat#ab-18356; RRID: AB_444447
Anti-H3	Abcam	Cat#ab-12079; RRID: AB_298834
Anti-HA (3F10)	Roche	Cat#11867423001; RRID: AB_10094468
Anti-Flag (M2)	Sigma-Aldrich	Cat#F1804; RRID: AB_262044
Anti-tubulin	Sigma-Aldrich	Cat#T5168; RRID: AB_477579
Anti-KDM5A	Bethyl	Cat#A300-897A: RRID: AB_2234038
Anti-KDM4A	Bethyl	Cat#A300-861A; RRID: AB_069461
Anti-KDM5C	Novus Biological	Cat#NB100-55328; RRID n/a
Anti-Ku70	Santa Cruz	Cat#sc-1487; RRID: AB_632614
Anti-goat IgG HRP conjugated	Santa Cruz	Cat#sc-2020; RRID: AB_631728
Anti-GAPDH	GeneTex	Cat#GTX100118; RRID: AB_1080976
Alexa Fluor 488–conjugated goat anti-Rabbit	Thermo Fisher	Cat#A-11034; RRID: AB_2576217
Alexa Fluor 555–conjugated goat anti-mouse	Thermo Fisher	Cat#A32727; RRID: AB_2633276
Rhodamine red–conjugated goat anti-mouse	Thermo Fisher	Cat#R-6393; RRID: AB_2556550
IRDye 680RD –conjugated goat anti-mouse	LI-COR Biosciences	Cat#925-68070; RRID: AB_2651128
IRDye 800 CW –conjugated goat anti-rabbit	LI-COR Biosciences	Cat#925-32211; RRID: AB_2651127
Chemicals, Peptides, and Recombinant Proteins		
JIB-04	Synthesized in-house (Wang et al., 2013)	N/A
GSK-J4	Tocris Bioscience	Cat#4594
GSK-J5	Tocris Bioscience	Cat#4689
PBIT	Sigma-Aldrich	Cat#PH009215
I-SceI enzyme	New England Bio Labs	Cat#R0694L
Critical Commercial Assays		
Ingenio Electroporation kit	Mirus Bio LLC	Cat#MIR 50115
H3K4me3 demethylation kit	Epigentek	Cat#P-3083
H3K9me3 demethylation kit	Epigentek	Cat#P-3081

REAGENT or RESOURCE	SOURCE	IDENTIFIER
EZ Magna ChIP A/G Chromatin Immunoprecipitation Kit	Millipore	Cat#17-100086
Experimental Models: Cell Lines		
U-2 OS	Dr. Sandeep Burma	N/A
LNCaP	Dr. Phil Thorpe	N/A
H1299	Dr. John D. Minna	N/A
A549	Dr. John D. Minna	N/A
HCC95	Dr. John D. Minna	N/A
HCC1195	Dr. John D. Minna	N/A
HCC2279	Dr. John D. Minna	N/A
HCC1719	Dr. John D. Minna	N/A
HBEC30KT	Dr. John D. Minna	N/A
HBEC3KT	Dr. John D. Minna	N/A
Experimental Models: Organisms/Strains		
Female athymic nude mice (nu/nu, 5–6 weeks old)	The Jackson Laboratory	Stock #: 002019
Oligonucleotides		
siRNA for Knock Down experiments	See Table S5	N/A
Oligonucleotides for RealTime Quantitative PCR	See Table S6	N/A
Recombinant DNA		
NHEJ-I reporter construct	Seluanov et al. (2010)	N/A
HR reporter construct	Seluanov et al. (2010)	N/A
Flag-KDM5B construct	Dr. Ralf Janknecht	N/A
HA-KDM5A construct	Addgene	plasmid #14799
HA-KDM4B construct	Addgene	plasmid #24181
HA-KDM4A construct	Dr. Yang Shi	N/A
Software and Algorithms		
ImageJ	NIH	https://imagej.nih.gov/ij/download.html
CellProfiler	Broad Institute	http://cellprofiler.org/releases/

CONTACT FOR REAGENT AND RESOURCE SHARING

Further information and requests for resources and reagents should be directed to and will be fulfilled by the Lead Contact, Elisabeth D. Martinez (elisabeth.martinez@utsouthwestern.edu).

EXPERIMENTAL MODEL AND SUBJECT DETAILS

Cell Lines—Human NSCLCs cell lines and immortalized non-cancerous human bronchial epithelial cells were kindly provided by Dr. John D. Minna. H1299 (male), A549 (male), HCC1719 (male), HCC95 (male), HCC1195 (male), HCC2270 (female) cancer cell lines were maintained in RPMI media with 5% fetal bovine serum. HBEC30KT (female) and

HBEC3KT (female) human bronchial epithelial cells were cultured in KSFM media with EGF and pituitary extract (KSFM supplements from GIBCO) in a humidified 37C incubator with 5% CO_2. U-2 OS (female) cells were kindly provided by Dr. S. Burma and maintained in DMEM media with 10% of FBS. LNCaP (male) cells, a gift of the late Phil Thorpe, were cultured in RPMI media supplemented with 10% FBS and penicillin-streptomycin. All cell lines were verified by DNA fingerprinting with the Promega Fusion system (Cat# DC2408) which consists of 24 short tandem repeat (STR) markers. These loci collectively provide a genetic profile with a random match probability of 6 3 10^{29}. Fingerprints were compared against our database of more than 2000 reference fingerprints which were collected from ATCC, DSMZ, JCRB, and RIKEN (Capes-Davis et al., 2013) and from our own resources (Gazdar et al., 2010). A match is called between two fingerprints when at least 80% of the alleles are identical according to the shared allele match algorithm defined by ICLAC. Mycoplasma contamination was tested periodically using e-Myco Mycoplasma PCR dectection kit (iNtRON Biotechnology, 25235).

Mice—Athymic nude mice female mice between 5 to 6 weeks were maintained with normal diet under standard animal housing condition. Animal experiments were carried out under approved IACUC protocols and followed UTSW animal care procedures (protocol number: APN2017–102260). NSCLC cells were injected subcutaneously (5 3 10^6 cells in 100 mL PBS H1299, 2 3 10^6 in 100 mL PBS A549 cells) into the right posterior leg of mice. Treatment was initiated when the subcutaneous tumors reached an average size of 150 to 200 mm^3. Mice were treated with JIB-04 (50 mg/kg/day) by oral gavage or with vehicle (12.5% Cremophor EL, 12.5% DMSO as an aqueous suspension); radiation was administered 4 hours after treatment. The treatment regimen consisted of a total of 12 doses of drug and/or IR given every other day. Tumor growth delay and the dose enhancement factor (DEF) were then determined. Body weight and general health were monitored every other day. Standard survival criteria was applied including severe lethargy, 20% weight loss, tumor burden > 2,000 mm^3 and/or difficulty breathing. Survival data was analyzed using GraphPad Prism software. All differences between treatment groups were analyzed by two-way ANOVA. For demethylase assays, animals were sacrificed 16 h after the last dose of treatment and tumors harvested and frozen.

METHOD DETAILS

Colony formation assays—Clonogenic cell survival of cells treated with IR alone or in combination with Jumonji inhibitors JIB-04, GSKJ-4, or PBIT, was analyzed by standard colony formation assays. JIB-04 Z-isomer, GSK-J5 and DMSO were used as controls. Cells were serially diluted to appropriate concentrations as shown in Table S4 and plated into 60-mm dishes in triplicate and allowed to attach for 4 h. Then cells were treated with the indicated drugs and irradiated 4 h later with graded doses of radiation for concurrent treatment (all experiments except Figure S1C), or irradiated first and 4 h later drugs added for post-treatment for comparison (Figure S1C). All cells were irradiated at room temperature in ambient air using a 137 Cs source (Mark 1–68 irradiator, JL Shepherd & Associated). Surviving colonies were stained with crystal violet 10 to 14 days later and colonies larger than approximately 50 cells were counted. The surviving clonogenic fraction of irradiated cells was normalized to the plating efficiency of un-irradiated controls. The data

are presented as the mean ± SD. The curve $S = e^{(aD + bD2)}$ was fitted to the experimental data using a least square fit algorithm with Sigma Plot 11.0 (Systat Software, Inc.). Inhibitor alone treatments were used to set the surviving fraction at 1.

Immunofluorescence staining—NSCLCs were seeded onto Lab-Tek II Chamber Slides (Thermo Fisher) and 24 hours later pretreated with JIB-04 or DMSO for 4 h. Then cells were exposed to a total dose of 2 Gy (γH2AX and 53BP1) or 10 Gy (RAD51 and DNAPKcs p-T2609) radiation. Cells were fixed in 4% formaldehyde/PBS for 15 min, permeabilized with 0.5% Triton X-100 for 15 min on ice, and blocked with 5% bovine serum albumin in PBS for 1 h. The slides were incubated with an antibody against phospho-Histone γH2AX (1:1000, 3 h at room temperature), 53BP1 (1:500, 3 h at room temperature), Rad-51 (1:500, 48 h 4C) or DNAPKcs p-T2609 (1:500, 48 h 4C). Alexa Fluor 488–conjugated goat anti-Rabbit, Alexa Fluor 555–conjugated goat anti-mouse or rhodamine red–conjugated goat anti-mouse secondary antibodies were used (1:1000, 1h at room temperature). Slides were mounted in a Vectashield mounting medium containing 4^0,6-diamidino-2-phenylindole (DAPI). Cells were imaged on a Zeiss upright fluorescent microscope. Foci counting was performed on the resulting images using the CellProfiler (CellProfiler.org) open-source cell image analysis software (algorithm available upon request) in a blinded fashion. Quantification was validated in several cases manually with ImageJ in a blinded fashion by two independent investigators.

Knockdown and overexpression studies—3×10^6 cells were transfected by electroporation using the Amaxa Nucleofector (program X-005) and the Ingenio Electroporation kit. For knock down experiments, cells were transfected with siRNA duplexes targeting the corresponding Jumonji enzyme or scrambled siRNA mixes with 250 nM final concentration. Knock down siRNA were from Sigma-Aldrich or QIAGEN and are summarized in Table S5. Knock-down cells were cultured for 48h before quantification of expression or further assays. For overexpression experiments, cells were transfected with pCMVHA-KDM4A, pCMVHA-KDM4B, pCMVHA-KDM5A, pCMVHA-KDM5B, or pcDNA3 plasmids (3mg), then allowed to recover in culture for 24h before proceeding with measurements of expression or further assays.

Western blot analysis—H1299 cells were transfected with siRNA or expression plasmids as above, harvested in RIPA buffer containing PhosSTOP 1× (Roche) and proteinase inhibitor cOmplete ULTRA Tablets, (Roche), the debris was pelleted (20,000 RCF x 15 min), protein quantified and equal amounts of protein run on SDS acrylamide gels. Protein was transferred to nitrocellulose or PVDF membranes and blotted using the indicated antibodies. Gels were imaged using using Odyssey infrared imaging or Li-Cor Odyssey Fc systems.

Quantitative RT-PCR—RNA of H1299 cells transfected with siRNA or expressing plasmids was extracted with RNeasy technology (QIAGEN). RNA was quantified, DNase treated and reverse transcribed. The cDNA was then amplified with Sybr green chemistry in real time quantitative PCR assays (Applied Biosystems) using validated primers specific for the human genes of interest. Reactions were performed on an ABI Prism 7900HT, with an

initial 2 min pre-incubation at 50C, followed by 10 min at 95C and then 40 cycles of 95C for 15 s and 60C for 1 min. 18S ribosomal RNA and cyclophilin were used as reference genes as before (Wang et al., 2013). Data were analyzed using the DDCt method (Bookout et al., 2006). Gene expression levels were then expressed as fold-induction over untransfected control cells. Reactions were run in triplicate and error bars represent experimental error, unless otherwise specified. Several distinct biological replicates were analyzed with equivalent results. Primer sequences are given in Table S6.

NHEJ and HR assays—The green fluorescent protein repair assay was performed as described by Seluanov et al. (2010). To generate reporter cell lines, 2 million H1299 cells were transfected with 0.5 mg of linearized NHEJ-I, or HR reporter constructs using the Amaxa Nucleofector program X-005. G418, at 1mg/ml, was added to the media 1 day post-transfection and stably transfected populations used two weeks post selection. Then transient expression of the I-SceI endonuclease was used to generate a DNA DSB at the integrated GFP gene sequences. Briefly, H1299 cells containing the NHEJ or the HR constructs treated for 4 h with JIB-04 or DMSO were transfected with the pCMV3×nls-I-SceI (5 mg, functional endonuclease) and a pN1-mCherry plasmid (0.05 mg) as transfection control as previously stated. To measure NHEJ and HR, cells were harvested, resuspended in 1 mL 1×PBS, put on ice, and analyzed on a BD FACScan instrument for GFP and mCherry expression. GFP and mCherry fluorescence was quantified using FlowJo software. DNA repair efficiency was calculated from the number of GFP-positive cells divided by the number of mCherry-positive cells. For the extrachromosomal assay in U-2 OS cells, NHEJ-I and HR plasmids were in vitro linearized by digestion with the I-SceI enzyme (NEB). Then, 1 million U-2 OS cells were transfected with 0.25 mg and 0.5 mg respectively of the linearized plasmids and the pN1-mCherry plasmid (0.025 mg) using the Amaxa Nucleofector program X-001. Cells were seeded in the presence of 800 nM JIB-04. Finally, 12 h and 24 h after seeding, DNA repair was analyzed as described above for H1299 stably transfected cells.

Cell cycle analysis—250,000 NSCLCs were seeded in 6 wells plates, 24 h latter cells were pretreated with JIB-04 as indicated or DMSO for 4 h and exposed to a total dose of 2 Gy. Then cells were collected 15min, 6 h or 12 h post IR and fixed using 75% ethanol at 20C for a minimum of 24 hours. The fixed cells were resuspended in PBS and incubated with 20 mL 1 mg/ml RNase A (Sigma) and 25 mg ml/ml propidium iodide (Sigma) for 30 min at room temperature. Experiments were done in triplicate. 20,000 cells were counted and the proportion of cells in different cell cycle phases was analyzed using the software Flowjo.

Histone demethylase activity assay—For histone demethylase activity determination in cells, 2×10^6 H1299 cells were seeded in P150 plates. After 24 h, cells were pretreated with indicated dose of JIB-04 or DMSO for 4h, irradiated with 8 Gy of radiation in a single dose. Note that the cell number/ density and amount of IR used was higher for demethylase assays than for radiation response curves which are based on low density colony formation assays or for foci resolution slides. Enzyme activity was not detectable at the lower cell numbers and thus both cell number and IR dose were increased to obtain similar levels of

DNA damage per cell area. Cells were harvested 15 min after IR and pellets resuspended in cold PBS containing PhosSTOP 1× (Roche), cOmplete ULTRA Tablets, EDTA-free, 1× (Roche) and 1 mM Wortmannin (Sigma-Aldrich). Cell suspensions were sonicated (3× 4 s, Ultrasonic Processor XL Sonicator), debris pelleted (15 min at 20,000 rcf.). For tumor extract preparation, tissues were collected 16 h after last dose of radiation and frozen. Twenty to 50 mg of frozen tumor tissue was dissociated in cold PBS supplemented as above with 2× EDTA-free protease inhibitors and 10 mM Wortmannin then then homologized by ultra-sonication using a TissueLyserII (QIAGEN, 2× 1min at 0.03/sec frequency). Supernatants after centrifugation (18,000 g for 10 min) were snap-freezed in liquid nitrogen until analysis. Protein in lysates were quantified, and equal amounts of protein (2.5 mg for cell extracts or 8.0 mg for tumor extracts) were incubated with a histone H3K4me3 or H3K9me3 substrate in a reaction buffer containing 50 mM HEPES pH 7.5, 0.01% Tween 20, 5 mM $(NH4)_2Fe(SO4)_2$ for cell extracts only, 1 mM a-ketoglutarate and 2 mM sodium L-ascorbate for 1 h at 37C. Specific immune-detection of the H3K4me2 or H3K9me2 product was measured using the Epigentek kit P-3083 for H3K4me3 demethylation or P-3081 for H3K9me3 demethylation. Background readings were given by heat inactivated extracts.

Immunoprecipitation—For γH2AX immunoprecipitation 1 3 10^7 H1299 cells were seeded in P150 plates. Next day cells were preincubated with 300 nM JIB04 for 4 h and then irradiated with 20 Gy. Due to the higher density of cells needed to obtain sufficient material to immunoprecipitate, we increased both JIB-04 dose and IR dose to obtain similar level of damage and KDM inhibition in the dense culture. Media was removed from cells, cells washed with PBS and fixed with 3% w/v PFA, 2% w/v sucrose in PBS for 1 min. Then cells were washed, scraped into media, pelleted by centrifugation (at 500×g for 2 min) and washed with cold PBS containing PhosSTOP 1× (Roche), cOmplete ULTRA Tablets, EDTA-free, 1× (Roche) and 1 mM Wortmannin (WM, Sigma-Aldrich). Cell pellets were re-suspended in 2.5 3 the packed cell volume of Nucleosome Preparation Buffer (NPB, 10mM HEPES [pH 7.9], 10 mMKCl, 1.0 mM $CaCl_2$, 1.5 mM $MgCl_2$, 0.34 M sucrose, 10% glycerol, 1mMDTT, 0.1% Triton X-100) containing PhosSTOP 1× (Roche), cOmplete ULTRA Tablets, EDTA-free, 1× (Roche), 1 mM Wortmannin (WM, Sigma-Aldrich) and 100 U ml1 micrococcal nuclease (MNase), and incubated at 37C for 45 min (note: WM is required to block in vitro DNA-PK/ATM activation by MNase-produced DSBs). An equal volume of Nucleosome Solubilization Buffer (NSB = NPB + 2% [v/v] NP-40, 2% [v/v] Triton X-100, 600 mMNaCl) was then added. Samples were vortexed, sonicated briefly and centrifuged at 10,000 rpm for 10 min. Protein levels were quantified, and 2 mg of the resulting supernatants were incubated with 2 ml of anti-γH2AX monoclonal antibody overnight at 4C with rotation. Immunocomplexes were pulled down by adding 45 ml of protein G-Sepharose for 3 h at 4C, washed three times with wash buffer (1× NPB + 1 X NSB), resuspended in 2× SDS sample buffer and incubated at 75C for 2 h to reverse cross-links. Equal amounts of protein run on 4%–12% SDS acrylamide gels. Protein was transferred to nitrocellulose membranes and blotted for phospho-Histone γH2AX (Ser139), Ku-70, H3K4me3 and H3K9me3. IRDye 680RD and IRDye 800 CW (LI-COR Biosciences) or and HRP-conjugated secondary antibodies were used and images captured with the

Odyssey infrared imaging system. Quantification was done using ImageJ or Image Studio Lite v5.2 software.

Chromatin immunoprecipitation/Re-precipitation—H1299 harboring the NHEJ construct were plated at 10^7 cells/P150 for 17–18 h then treated with DMSO or JIB-04 (300 nM) for 4 h. Cells were trypsinized and transfected with pCMV3×nls-I-SceI (5 mg plasmid/ 3×10^6 cells/electroporation reaction as stated above). After electroporation, cells were plated at 10^7 cells/P150 with continued treatment to allow for I-SceI expression. 19–20 h later cells were collected, fixed, washed and resuspended in NBP as stated for immunoprecipitation of γH2AX. Chromatin was generated by adding 17 units of MNase/ mL and incubated at 37C for 30 min. The reactions were stopped by EDTA (70 mM final concentration). Nuclei were collected by spinning at 16,000 g for 10 minutes at 4C. Buffers used for ChIP, reChIP and protein A/G beads came from the EZ Magna ChIP kit (Millipore 17–100086) unless stated. Nuclei pellets were dissolved in 2.5 3 the packed cell volume in SDS ChIP lysis buffer supplemented with phosphatase and proteinase inhibitors and Wortmanin as above. Chromatin solutions were rolled at 4C for 10 min, the insoluble materials were removed by spinning at 21,000 g for 10 min. 800 mg of protein was used per ChIP reaction. For ChIP, 15 uL of 1 mg/mL of γH2AX antibody was used per reaction except in parallel no antibody controls. Lysates were incubated with agitation at 4C overnight. Protein A/G beads were added and incubated with agitation for 2–3 hours at 4C. Beads were collected and washed according to the manufacture's instruction. ChIP products were eluted from the beads using 300 mL of ReChIP elution buffer (2% SDS, 15 mM DTT in TE) with agitation at 37C for 1 h. 150 mL was diluted 21 times in reChIP dilution buffer (30ug/mL BSA in ChIP dilution buffer) supplemented as before. The re-ChIP solutions were precleared with protein A/G then split into two parts. 8 mL of H3K4me3 antibody or no antibody were added. Both tubes were incubated overnight with agitation at 4C and processed as in the ChIP steps. re-ChIP products were eluted from the beads using 250 mL of ChIP elution buffer (1% SDS in 100 mM $NaHCO_3$) twice at room temperature with agitation. re-ChIP inputs and re-ChIP eluates were brought up to 500 mL with ChIP elution buffer and uncross-linked at 65C overnight with 200 mM NaCl. Samples were treated with DNase free RNase (1 mL of 10 mg/mL for 30 min at 37C) followed by proteinase K (1 mL of 20 mg/mL at 45C for 1 h) in the presence of 10 mM of EDTA and 40 mM Tris, pH6.5. DNA was purified using Phenol:Chloroform:Isoamyl alcohol extraction and quantified by qPCR using validated primers (see Table S6). The control genomic primer has been previously characterized (Aymard et al., 2014).

TCGA Analysis—Clinical information and gene expression (RNA-Seq) data were obtained from The Cancer Genome Atlas (TCGA) for lung squamous cell carcinoma (LUSC). The gene expression of Jumonji genes from radiated patients with complete response (defined as radiosensitive) were compared with radiated patients with radiographic progressive disease or partial response (defined as radioresistant) using t tests controlling for the equality of variances as described (Peñ a-Llopis et al., 2011).

QUANTIFICATION AND STATISTICAL ANALYSES

All numerical results are reported as mean ± standard error of the mean (SEM) or as mean + standard deviation (SD). Unless otherwise specified, unpaired 2-sided Student's t test, one-way analysis of variance followed by post-tests, Kruskal-Wallis or Dunn's (GraphPad Prism Software), were used for statistical analyses, as indicated. Clonogenic survival curves were modeled with the linear quadratic equation ($S = e^{[aD + bD2]}$) for radiation treatment and a four-parameter variable slope regression for drug toxicity. Differences with p values lower than 0.05 were considered as statistically significant. The exact statistical analyses used, the significance value, the sample size (n) and number of biological replicates are indicated in each figure or figure legend.

Supplementary Material

Refer to Web version on PubMed Central for supplementary material.

ACKNOWLEDGMENTS

We are grateful to Dr. S. Burma for suggestions, reagents, and critical reading of the manuscript. We thank Dr. D. Saha for insightful input for the design of the *in vivo* studies. We are grateful to Dr. John D. Minna for helpful suggestions and cell lines. We acknowledge GFP plasmids for NHEJ and HR from Dr. V. Gorb-unova. We thank Christopher Gonzales and Kossi Senagbe for technical assistance. This work was supported by the NCI (R01 CA125269 and SPORE grant P50CA70907), a DoD Concept award (W81×WH-16–1-0129), by CPRIT (RP120717 and RP160493), the Friends of the Cancer Center at UTSW, and The Welch Foundation (I-1878). We are grateful for support from the NCT-Hei-delberg School of Oncology Program.

REFERENCES

Amendola PG, Zaghet N, Ramalho JJ, Vilstrup Johansen J, Boxem M, and Salcini AE (2017). JMJD-5/KDM8 regulates H3K36me2 and is required for late steps of homologous recombination and genome integrity. PLoS Genet. 13, e1006632. [PubMed: 28207814]

Anscher MS (2010). Targeting the TGF-beta1 pathway to prevent normal tissue injury after cancer therapy. Oncologist 15, 350–359. [PubMed: 20413640]

Aymard F, Bugler B, Schmidt CK, Guillou E, Caron P, Briois S, Iacovoni JS, Daburon V, Miller KM, Jackson SP, and Legube G (2014). Transcriptionally active chromatin recruits homologous recombination at DNA double-strand breaks. Nat. Struct. Mol. Biol 21, 366–374. [PubMed: 24658350]

Bayo J, Dalvi MP, and Martinez ED (2015). Successful strategies in the discovery of small-molecule epigenetic modulators with anticancer potential. Future Med. Chem 7, 2243–2261. [PubMed: 26510529]

Bookout AL, Cummins CL, Mangelsdorf DJ, Pesola JM, and Kramer MF (2006). High-throughput real-time quantitative reverse transcription PCR. Curr. Protoc. Mol. Biol Chapter 15, Unit 15.18.

Burgess RC, Burman B, Kruhlak MJ, and Misteli T (2014). Activation of DNA damage response signaling by condensed chromatin. Cell Rep. 9, 1703–1717. [PubMed: 25464843]

Cao LL, Wei F, Du Y, Song B, Wang D, Shen C, Lu X, Cao Z, Yang Q, Gao Y, et al. (2016). ATM-mediated KDM2A phosphorylation is required for the DNA damage repair. Oncogene 35, 301–313. [PubMed: 25823024]

Capes-Davis A, Reid YA, Kline MC, Storts DR, Strauss E, Dirks WG, Drexler HG, MacLeod RA, Sykes G, Kohara A, et al. (2013). Match criteria for human cell line authentication: where do we draw the line? Int. J.Cancer 132, 2510–2519. [PubMed: 23136038]

Chapman JR, Taylor MR, and Boulton SJ (2012). Playing the end game: DNA double-strand break repair pathway choice. Mol. Cell 47, 497–510. [PubMed: 22920291]

Chen L, Fu L, Kong X, Xu J, Wang Z, Ma X, Akiyama Y, Chen Y, and Fang J (2014). Jumonji domain-containing protein 2B silencing induces DNA damage response via STAT3 pathway in colorectal cancer. Br. J. Cancer 110, 1014–1026. [PubMed: 24473398]

Chiolo I, Tang J, Georgescu W, and Costes SV (2013). Nuclear dynamics of radiation-induced foci in euchromatin and heterochromatin. Mutat. Res750, 56–66. [PubMed: 23958412]

Crino` L, Weder W, van Meerbeeck J, Felip E, and Group EGW; ESMO Guidelines Working Group (2010). Early stage and locally advanced (non-metastatic) non-small-cell lung cancer: ESMO Clinical Practice Guidelines for diagnosis, treatment and follow-up. Ann. Oncol 21 (Suppl 5), v103–v115. [PubMed: 20555058]

Dalvi MP, Wang L, Zhong R, Kollipara RK, Park H, Bayo J, Yenerall P, Zhou Y, Timmons BC, Rodriguez-Canales J, et al. (2017). Taxaneplatin-resistant lung cancers co-develop hypersensitivity to JumonjiC demethylase inhibitors. Cell Rep. 19, 1669–1684. [PubMed: 28538184]

Das AK, Bell MH, Nirodi CS, Story MD, and Minna JD (2010). Radiogenomics predicting tumor responses to radiotherapy in lung cancer. Semin.Radiat. Oncol 20, 149–155. [PubMed: 20685577]

Eberhardt W, Po¨ ttgen C, and Stuschke M. (2006). Chemoradiation paradigm for the treatment of lung cancer. Nat. Clin. Pract. Oncol 3, 188–199. [PubMed: 16596143]

Falkson CB, Vella ET, Yu E, El-Mallah M, Mackenzie R, Ellis PM, and Ung YC (2017). Guideline for radiotherapy with curative intent in patients with early-stage medically inoperable non-small-cell lung cancer. Curr. Oncol 24, e44–e49. [PubMed: 28270731]

Firsanov DV, Solovjeva LV, and Svetlova MP (2011). H2AX phosphorylation at the sites of DNA double-strand breaks in cultivated mammalian cells and tissues. Clin. Epigenetics 2, 283–297. [PubMed: 22704343]

Fnu S, Williamson EA, De Haro LP, Brenneman M, Wray J, Shaheen M, Radhakrishnan K, Lee SH, Nickoloff JA, and Hromas R (2011). Methylation of histone H3 lysine 36 enhances DNA repair by nonhomologous end-joining. Proc. Natl. Acad. Sci. USA 108, 540–545. [PubMed: 21187428]

Gazdar AF, Girard L, Lockwood WW, Lam WL, and Minna JD (2010). Lung cancer cell lines as tools for biomedical discovery and research. J. Natl. Cancer Inst 102, 1310–1321. [PubMed: 20679594]

Gil del Alcazar CR, Hardebeck MC, Mukherjee B, Tomimatsu N, Gao X, Yan J, Xie XJ, Bachoo R, Li L, Habib AA, and Burma S (2014). Inhibition of DNA double-strand break repair by the dual PI3K/mTOR inhibitor NVPBEZ235 as a strategy for radiosensitization of glioblastoma. Clin. Cancer Res20, 1235–1248. [PubMed: 24366691]

Gil Del Alcazar CR, Todorova PK, Habib AA, Mukherjee B, and Burma S (2016). Augmented HR repair mediates acquired temozolomide resistance in glioblastoma. Mol. Cancer Res 14, 928–940. [PubMed: 27358111]

Goodarzi AA, Noon AT, Deckbar D, Ziv Y, Shiloh Y, Lo¨ brich M, and Jeggo PA. (2008). ATM signaling facilitates repair of DNA double-strand breaks associated with heterochromatin. Mol. Cell 31, 167–177. [PubMed: 18657500]

Howington JA, Blum MG, Chang AC, Balekian AA, and Murthy SC (2013). Treatment of stage I and II non-small cell lung cancer: diagnosis and management of lung cancer, 3rd ed: American College of Chest Physicians evidence-based clinical practice guidelines. Chest 143, e278S–e313S. [PubMed: 23649443]

Hunt CR, Ramnarain D, Horikoshi N, Iyengar P, Pandita RK, Shay JW, and Pandita TK (2013). Histone modifications and DNA double-strand break repair after exposure to ionizing radiations. Radiat. Res 179, 383–392. [PubMed: 23373901]

Iacovoni JS, Caron P, Lassadi I, Nicolas E, Massip L, Trouche D, and Legube G (2010). High-resolution profiling of gammaH2AX around DNA double strand breaks in the mammalian genome. EMBO J. 29, 1446–1457. [PubMed: 20360682]

Janssen A, Breuer GA, Brinkman EK, van der Meulen AI, Borden SV, van Steensel B, Bindra RS, LaRocque JR, and Karpen GH (2016). A single double-strand break system reveals repair dynamics and mechanisms in heterochromatin and euchromatin. Genes Dev. 30, 1645–1657. [PubMed: 27474442]

Jeggo PA, Geuting V, and Lo¨ brich M. (2011). The role of homologous recombination in radiation-induced double-strand break repair. Radiother. Oncol 101, 7–12. [PubMed: 21737170]

Karagiannis TC, and El-Osta A (2007). Chromatin modifications and DNA double-strand breaks: the current state of play. Leukemia 21, 195–200. [PubMed: 17151702]

Kinner A, Wu W, Staudt C, and Iliakis G (2008). Gamma-H2AX in recognition and signaling of DNA double-strand breaks in the context of chromatin. Nucleic Acids Res. 36, 5678–5694. [PubMed: 18772227]

Kruidenier L, Chung CW, Cheng Z, Liddle J, Che K, Joberty G, Bantscheff M, Bountra C, Bridges A, Diallo H, et al. (2012). A selective jumonji H3K27 demethylase inhibitor modulates the proinflammatory macrophage response. Nature 488, 404–408. [PubMed: 22842901]

Lesueur P, Chevalier F, Austry JB, Waissi W, Burckel H, Noe¨ l G, Habrand JL, Saintigny Y, and Joly F (2017). Poly-(ADP-ribose)-polymerase inhibitors as radiosensitizers: a systematic review of pre-clinical and clinical human studies. Oncotarget 8, 69105–69124. [PubMed: 28978184]

Li X, Liu L, Yang S, Song N, Zhou X, Gao J, Yu N, Shan L, Wang Q, Liang J, et al. (2014). Histone demethylase KDM5B is a key regulator of genome stability. Proc. Natl. Acad. Sci. USA 111, 7096–7101. [PubMed: 24778210]

Lin CS, Lin YC, Adebayo BO, Wu A, Chen JH, Peng YJ, Cheng MF, Lee WH, Hsiao M, Chao TY, and Yeh CT (2015). Silencing JARID1B suppresses oncogenicity, stemness and increases radiation sensitivity in human oral carcinoma. Cancer Lett. 368, 36–45. [PubMed: 26184998]

Mallette FA, Mattiroli F, Cui G, Young LC, Hendzel MJ, Mer G, Sixma TK, and Richard S (2012). RNF8- and RNF168-dependent degradation of KDM4A/JMJD2A triggers 53BP1 recruitment to DNA damage sites. EMBO J. 31, 1865–1878. [PubMed: 22373579]

Martinez ED, and Gazdar AF (2016). Inhibiting the Jumonji family: a potential new clinical approach to targeting aberrant epigenetic mechanisms. Epigenomics 8, 313–316. [PubMed: 26918824]

Pen˜ a-Llopis S, Vega-Rubin-de-Celis S, Schwartz JC, Wolff NC, Tran TA, Zou L, Xie XJ, Corey DR, and Brugarolas J. (2011). Regulation of TFEB and V-ATPases by mTORC1. EMBO J. 30, 3242–3258. [PubMed: 21804531]

Provencio M, and Sa´ nchez A. (2014). Therapeutic integration of new molecule-targeted therapies with radiotherapy in lung cancer. Transl. Lung Cancer Res 3, 89–94. [PubMed: 25806286]

Sato M, Vaughan MB, Girard L, Peyton M, Lee W, Shames DS, Ramirez RD, Sunaga N, Gazdar AF, Shay JW, and Minna JD (2006). Multiple oncogenic changes (K-RAS(V12), p53 knockdown, mutant EGFRs, p16 bypass, telomerase) are not sufficient to confer a full malignant phenotype on human bronchial epithelial cells. Cancer Res. 66, 2116–2128. [PubMed: 16489012]

Sato M, Larsen JE, Lee W, Sun H, Shames DS, Dalvi MP, Ramirez RD, Tang H, DiMaio JM, Gao B, et al. (2013). Human lung epithelial cells progressed to malignancy through specific oncogenic manipulations. Mol. Cancer Res 11, 638–650. [PubMed: 23449933]

Sayegh J, Cao J, Zou MR, Morales A, Blair LP, Norcia M, Hoyer D, Tackett AJ, Merkel JS, and Yan Q (2013). Identification of small molecule inhibitors of Jumonji AT-rich interactive domain 1B (JARID1B) histone demethylase by a sensitive high throughput screen. J. Biol. Chem 288, 9408–9417. [PubMed: 23408432]

Seiler DM, Rouquette J, Schmid VJ, Strickfaden H, Ottmann C, Drexler GA, Mazurek B, Greubel C, Hable V, Dollinger G, et al. (2011).Double-strand break-induced transcriptional silencing is associated with loss of tri-methylation at H3K4. Chromosome Res. 19, 883–899. [PubMed: 21987186]

Seluanov A, Mao Z, and Gorbunova V (2010). Analysis of DNA doublestrand break (DSB) repair in mammalian cells. J. Vis. Exp 43, 2002.

Solovjeva LV, Svetlova MP, Chagin VO, and Tomilin NV (2007). Inhibition of transcription at radiation-induced nuclear foci of phosphorylated histone H2AX in mammalian cells. Chromosome Res. 15, 787–797. [PubMed: 17874213]

Song SY, Das AK, and Minna JD (2014). Comparison between concurrent and sequential chemoradiation for non-small cell lung cancer in vitro. Oncol. Lett 7, 307–310. [PubMed: 24396437]

Tofilon PJ, and Camphausen K (2009). Molecular targets for tumor radiosensitization. Chem. Rev 109, 2974–2988. [PubMed: 19338375]

Tsouroula K, Furst A, Rogier M, Heyer V, Maglott-Roth A, Ferrand A, Reina-San-Martin B, and Soutoglou E (2016). Temporal and spatial uncoupling of DNA double strand break repair pathways within mammalian heterochromatin. Mol. Cell 63, 293–305. [PubMed: 27397684]

Ui A, Nagaura Y, and Yasui A (2015). Transcriptional elongation factor ENL phosphorylated by ATM recruits polycomb and switches off transcription for DSB repair. Mol. Cell 58, 468–482. [PubMed: 25921070]

Vinogradova M, Gehling VS, Gustafson A, Arora S, Tindell CA, Wilson C, Williamson KE, Guler GD, Gangurde P, Manieri W, et al. (2016). An inhibitor of KDM5 demethylases reduces survival of drug-tolerant cancer cells. Nat. Chem. Biol 12, 531–538. [PubMed: 27214401]

Wang L, Chang J, Varghese D, Dellinger M, Kumar S, Best AM, Ruiz J, Bruick R, Pen˜ a-Llopis S, Xu J, et al. (2013). A small molecule modulates Jumonji histone demethylase activity and selectively inhibits cancer growth. Nat. Commun 4, 2035. [PubMed: 23792809]

Ward JF (1988). DNA damage produced by ionizing radiation in mammalian cells: identities, mechanisms of formation, and reparability. Prog. Nucleic Acid Res. Mol. Biol 35, 95–125. [PubMed: 3065826]

Watanabe S, Watanabe K, Akimov V, Bartkova J, Blagoev B, Lukas J, and Bartek J (2013). JMJD1C demethylates MDC1 to regulate the RNF8 and BRCA1-mediated chromatin response to DNA breaks. Nat. Struct. Mol. Biol 20, 1425–1433. [PubMed: 24240613]

Wu X, Johansen JV, and Helin K (2013). Fbxl10/Kdm2b recruits polycomb repressive complex 1 to CpG islands and regulates H2A ubiquitylation. Mol. Cell 49, 1134–1146. [PubMed: 23395003]

Young LC, McDonald DW, and Hendzel MJ (2013). Kdm4b histone demethylase is a DNA damage response protein and confers a survival advantage following g-irradiation. J. Biol. Chem 288, 21376–21388. [PubMed: 23744078]

Zheng H, Chen L, Pledger WJ, Fang J, and Chen J (2014). p53 promotes repair of heterochromatin DNA by regulating JMJD2b and SUV39H1 expression. Oncogene 33, 734–744. [PubMed: 23376847]

Highlights

- Inhibition of JARID demethylases sensitizes cancers to radiation in vitro and *in vivo*
- Radiotherapy increases JARID enzyme activity, and blocking it prevents DNA repair
- H3K4me3 accumulates at and near DSBs and impedes recruitment of DNA repair factors
- Human tumors with high levels of JARID1B expression are resistant to radiotherapy

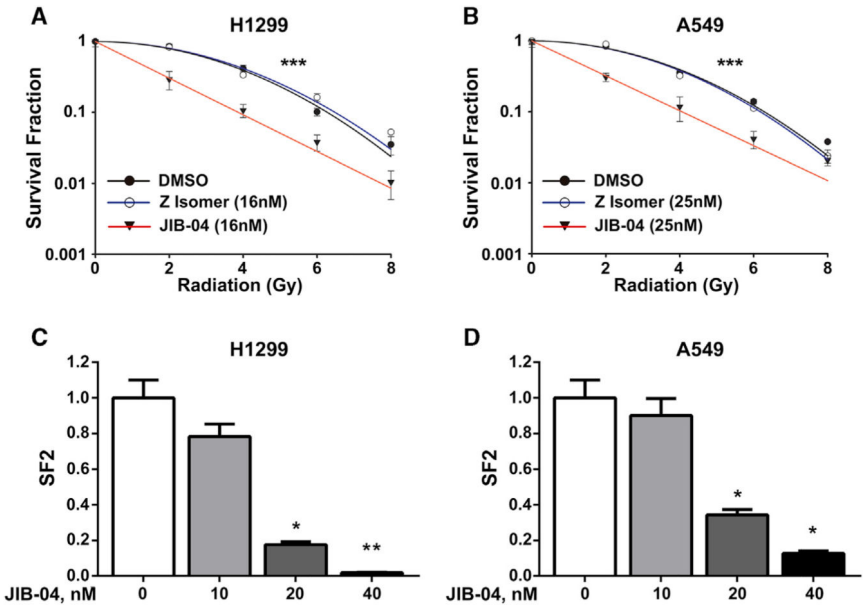

Figure 1. JIB-04 Robustly Sensitizes Radioresistant NSCLC to IR

(A and B) Clonogenic survival of H1299 (A) or A549 (B) cells treated with 16 nM or 25 nM JIB-04, respectively, and then irradiated as indicated (0–8 Gy). The survival of cells treated with JIB-04 alone was set to 1. Graphs show one of two independent experiments, each done in triplicate. Error bars represent SD across triplicates. ***$p < 0.001$, DMSO or Z-isomer versus JIB-04 (A) (2-way ANOVA); ***$p < 0.001$, DMSO or Z-isomer versus JIB-04 (2 way ANOVA).

(C and D) Clonogenic survival of H1299 (C) and A549 (D) cells treated with increasing doses of JIB04 (0–40 nM) and 2 Gy IR. The number of colonies was normalized to the colonies formed by cells treated with the corresponding dose of JIB-04 alone (without IR). Graph represents one of two experiments (n = 3). Error bars show SD. *$p < 0.05$; **$p < 0.01$ versus vehicle (0 nM) (Kruskal-Wallis).

See also Figure S1 and Table S1.

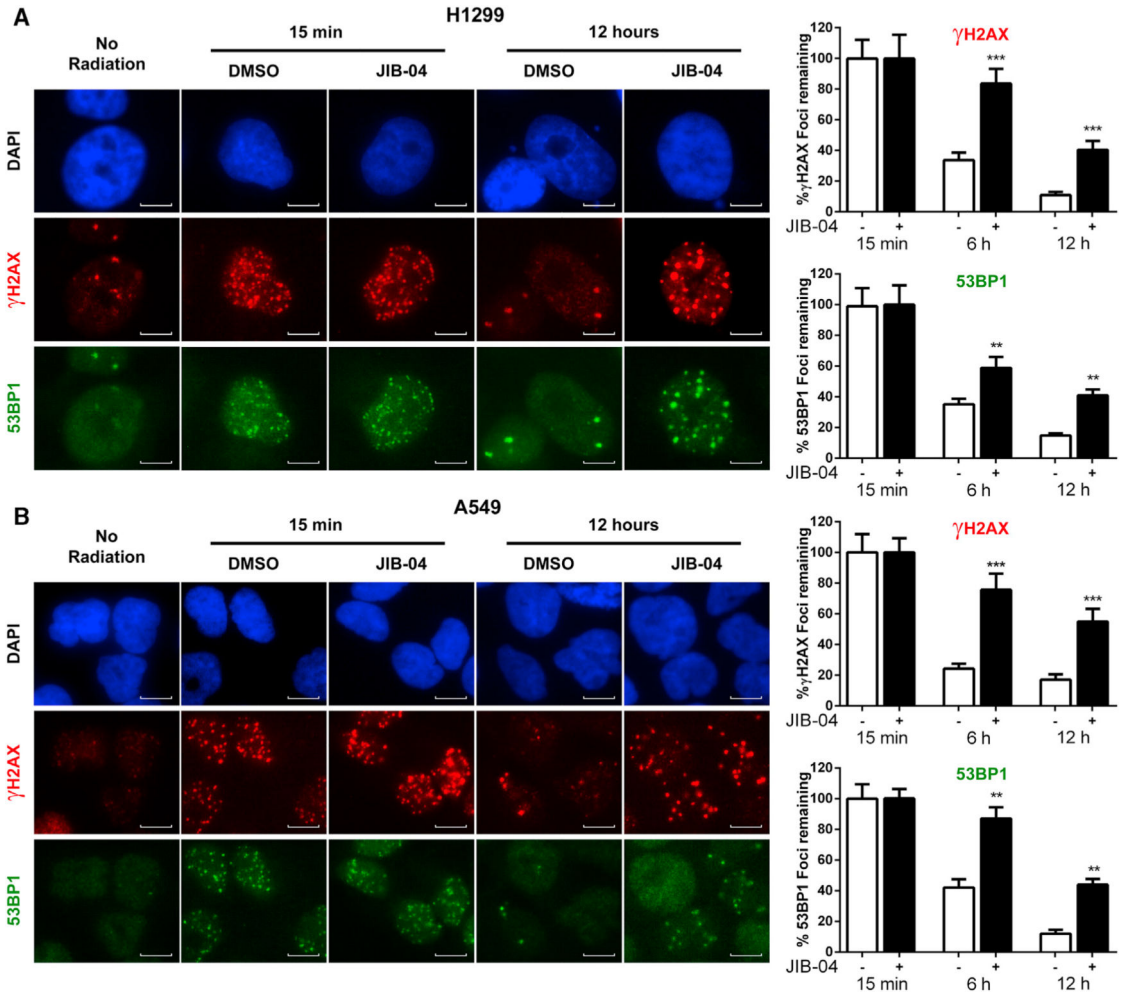

Figure 2. Defective Resolution of γH2AX and 53BP1 Foci in JIB-04-Treated Cells

(A and B) DNA DSB repair kinetics after IR in H1299 (A) and A549 (B) cells. Cells were incubated with DMSO vehicle or JIB-04 for 4 hr (16 nM for H1299 and 25 nM for A549), irradiated (2 Gy), fixed at the indicated time points, and then immunostained for γH2AX (red) and 53BP1 (green). Scale bars, 10 μm. Foci per nucleus were counted (> 100 nuclei per treatment). Representative images are shown in the left panels for 15 min and 12 hr. Repair kinetics are plotted as the percentage + SEM of remaining foci against time in the right bar graphs for measured time points. ***$p < 0.001$; **$p < 0.01$ versus control (ANOVA). Representative data from one of three independent experiments are shown. See also Figures S2 and S3 and Table S2.

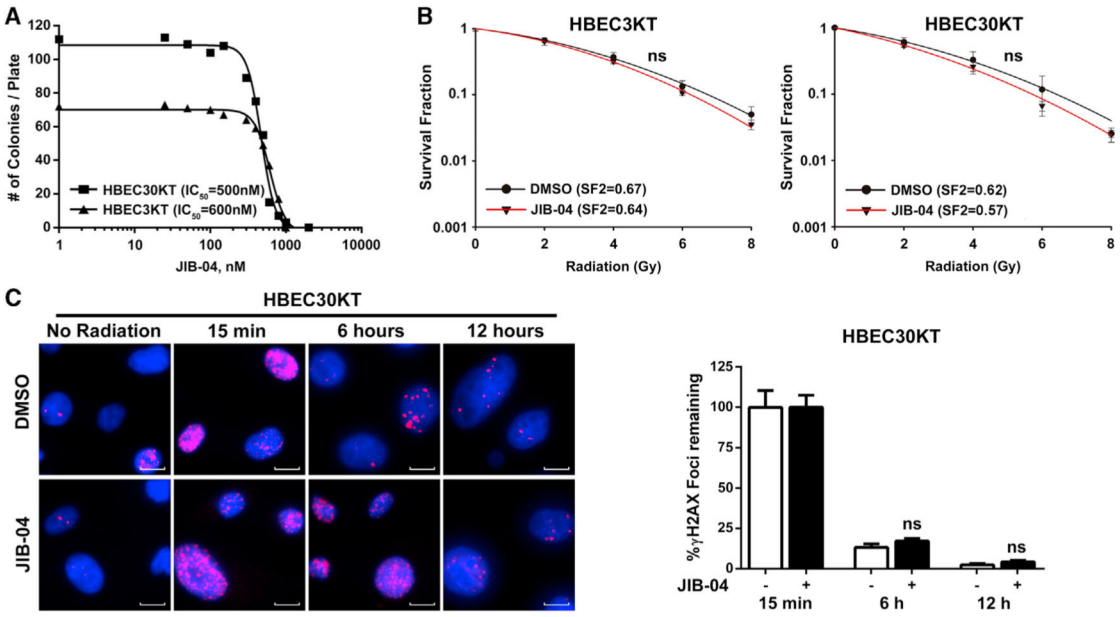

Figure 3. The Radiosensitizing Effects and DNA Repair Defects Induced by JIB-04 Are Cancer Selective

(A) JIB-04 IC_{50} determined by liquid colony formation in immortalized non-transformed human bronchial epithelial cells HBEC3KT and HBEC30KT. Graph represents one experiment done in triplicate.

(B) Clonogenic survival of HBEC3KT and HBEC30KT cells treated with 600 nM or 500 nM JIB-04, respectively, and then irradiated as indicated. Curves werederived as in Figure 1B. Graph represents one of three experiments done in triplicate. Values represent the average survival fraction ± SD of triplicate samples. ns indicates that no significant differences in radiosensitization curves across treatments were observed ($p \geq 0.1$, 2-way ANOVA).

(C) DNA DSB repair kinetics in HBEC30KT cells. Cells were incubated with vehicle or 500 nM JIB-04 for 4 hr, irradiated (2 Gy), fixed, immunostained for γH2AX, and then quantified as in Figure 2. Representative images are shown on the left panel. Scale bars, 10 μm. Repair kinetics are plotted in the right bar graphs as percentage + SEM of remaining foci over time. ns indicates that no significant differences were observed between vehicle and treatment groups at any time point ($p > 0.8$, ANOVA). Data are from >50 nuclei per treatment for one of two experiments.

See also Figure S3.

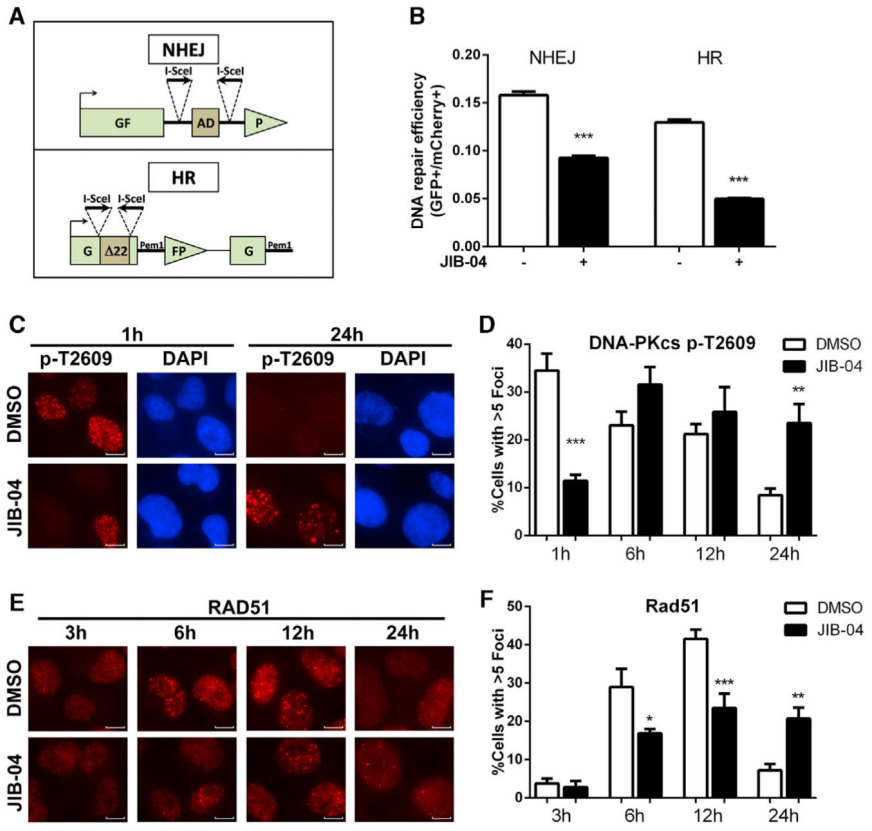

Figure 4. JIB-04 Inhibits Both NHEJ and HR Repair

(A) Schematic of the reporter constructs used inHR and NHEJ repair assays.

(B) H1299 cells stably containing the NHEJ or theHR constructs were treated with JIB-04 or DMSO for 4 hr and then transfected with the pCMV3×nls-I-*SceI* (functional endonuclease) and a pN1-mCherry plasmid as transfection control in the continuous presence of treatment (300 nM JIB-04). Cells were analyzed by flow cytometry for GFP and mCherry expression 24 hr after transfection. 20,000 cells were analyzed in each sample and NHEJ or HR repair frequency calculated (%GFP+ cells/%mCherry+ cells). Average + SEM values of triplicates for one of three representative experiments are shown. ***$p < 0.001$ versus vehicle control (Kruskal-Wallis).

(C–F) DNA-PKcs p-T2609 (C and D) and RAD51 (E and F) foci kinetics in H1299 cells. Cells were incubated with vehicle or 16 nM JIB-04 for 4 hr, irradiated (10 Gy), fixed, and immunostained, and then the number of foci per nucleus in >100 cells was counted for each time point. (C) and (E) show representative immunofluorescence images (scale bars, 10 μm), and (D) and (F) show foci formation and resolution kinetics obtained by plotting the percentage + SEM of cells with more than 5 foci per nucleus over time (***$p < 0.001$; **$p < 0.01$; *$p < 0.05$ versus DMSO control per time point [ANOVA]). Data are representative of one of two independent experiments.

See also Figure S5.

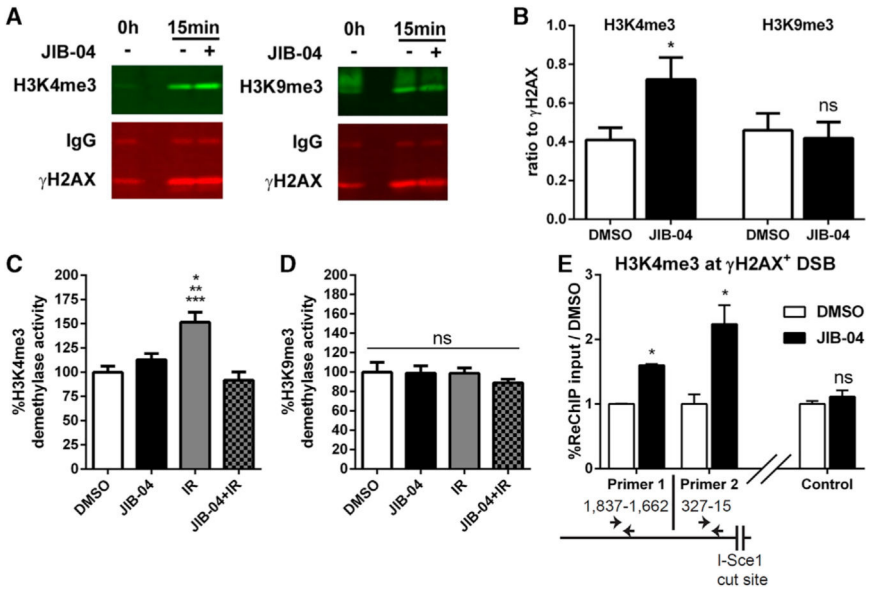

Figure 5. Jumonji Inhibition by JIB-04 Results in H3K4me3 Enrichment at DSBs

(A) Cells were incubated with vehicle or 300 nM JIB-04 for 4 hr, irradiated (20 Gy), and lysed, and nucleosomes were solubilized. γH2AX was immunoprecipitated from 2 mg soluble nucleosome extract and immune-precipitates blotted for γH2AX and H3K4me3 (left) or H3K9me3 (right).

(B) The immunoblot data from three independent experiments were quantified and expressed as the average ratio H3K4me3 signal/γH2AX signal or H3K9me3 signal/γH2AX signal + SEM. *$p < 0.05$; ns, not significant ($p = 0.74$); DMSO versus JIB-04(t test).

(C and D) H1299 cells were pretreated with JIB04 (16 nM) for 4 hr followed by IR (8 Gy) and collected at 15 min after radiation. Cellular extracts were prepared and H3K4me3 (C) and H3K9me3 (D) activity measured. Values in (C) and (D) are expressed as percentage + SEM ofDMSO-treated activity across three independent experiments. *$p < 0.05$ IR versus JIB-04; **$p < 0.001$ IR versus DMSO; ***$p < 0.001$ IR versus JIB-04+IR; ns, not significant ($p > 0.8$) (Kruskal-Wallis).

(E) H1299-NHEJ stable cells pretreated with DMSO or 300 nM JIB-04 were transfected with I-Sce1 plasmid to induce DSBs, and 20 hr later, ChIP/re-ChIP experiments were carried out by immunoprecipitating the product of γH2AX ChIP with H3K4me3 antibodies. Levels of associated DNA were measured by qPCR. *$p = 0.012$ (DMSO versus JIB-04 for primer 1); *$p = 0.011$ (DMSO versus JIB-04 for primer 2); ns, $p = 0.3$ (DMSO versus JIB-04 for control region) (onetailed paired t test). n = 2–4 replicates of one experiment; average percentage of re-ChIP input relative to DMSO ± SEM is shown.

See also Figure S6.

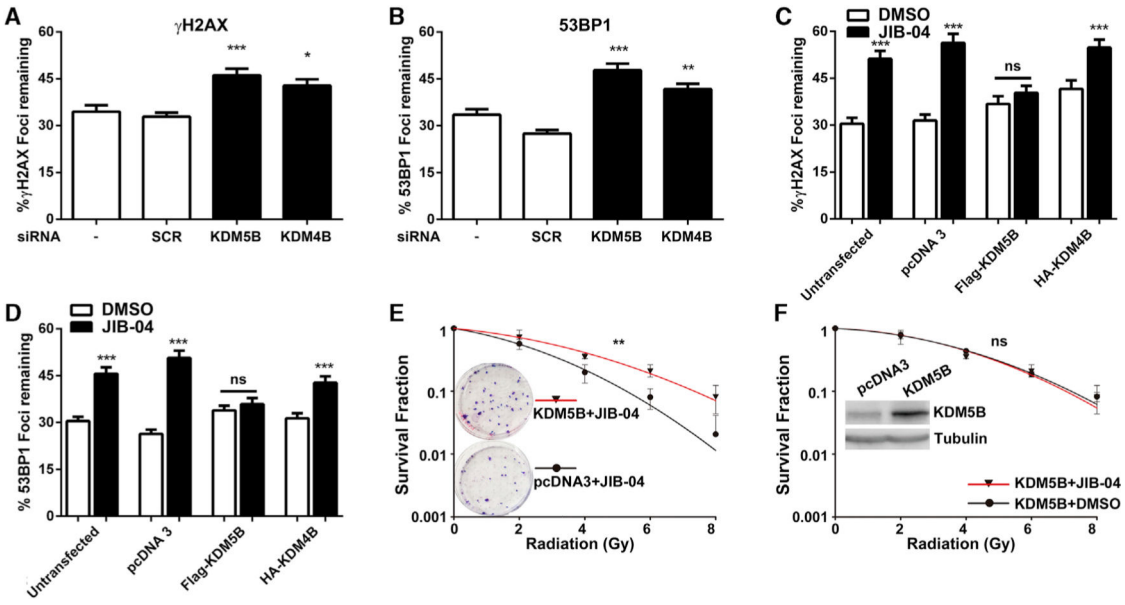

Figure 6. Jumonji Enzyme Knockdown Phenocopies the JIB-04 Repair Defect, and Overexpression of KDM5B Rescues the JIB-04-Induced DNA Repair Defects and Radiosensitization of Cancer Cells

(A and B) DNA DSB repair kinetics in H1299 cells after knockdown of KDM5B or KDM4B. Cells were irradiated 48 hr after transfection (2 Gy) and immunostained for γH2AX (A) and 53BP1 (B), and then the number of foci per nucleus were counted after 6 hr (>100 nuclei). Graphs represent the percent of foci remaining + SEM for one of three equivalent independent experiments. ***$p < 0.001$; **$p < 0.01$; *$p < 0.05$ versus controls (ANOVA).

(C and D) DNA DSB repair kinetics showing γH2AX (C) or 53BP1 (D) in H1299 cells overexpressing FLAG-KDM5B or HA-KDM4B. 24 hr after transfection, cells were incubated with 16 nM JIB-04 for 4 hr, irradiated (2 Gy), and processed as above. Graphs represent the percent of remaining foci + SEM 6 hr after radiation for one of three independent experiments. ***$p < 0.001$ versus controls; ns, $p > 0.4$ (ANOVA).

(E and F) Clonogenic survival of H1299 cells transfected with pcDNA3 empty vector or overexpressing KDM5B and treated with JIB-04 (E) or KDM5B-overexpressing cells treated with DMSO versus JIB-04 (F). **$p < 0.01$ KDM5B+JIB-04 versus pcDNA3+JIB-04; ns, no significant difference ($p = 0.5$) KDM5B+JIB-04 versus KDM5B+DMSO (2-way ANOVA). Inset in (E) shows representative images of colony assays of cells transfected with pcDNA3 or overexpressing KDM5B treated with JIB-04 and 8 Gy radiation. Inset in (F) is a western blot showing the overexpression of KDM5B in cells used for these studies. Data represent the average of three to four independent experiments. Error bars represent SD across experiments.

See also Figure S7.

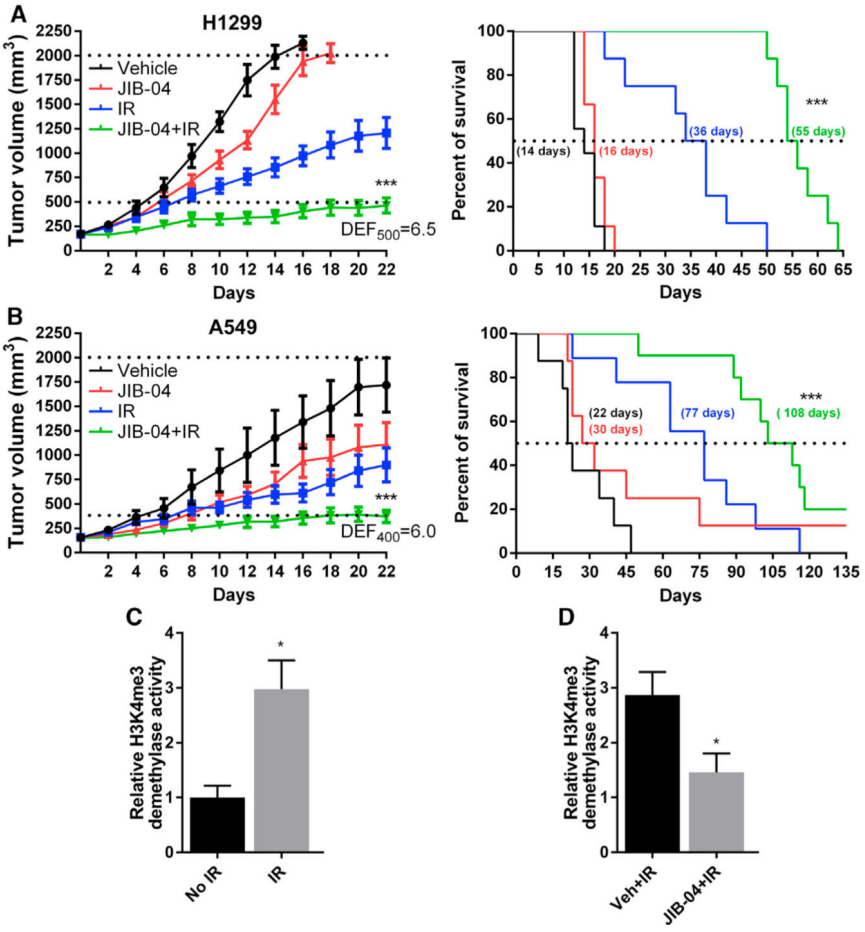

Figure 7. JIB-04 Robustly Radiosensitizes Tumors *In vivo* and Prolongs the Survival of Tumor-Bearing Mice

(A) Subcutaneous tumors generated from H1299 cells were allowed to reach a volume between 150 to 200 mm^3, and then mice were treated every other day with vehicle (n = 9), JIB-04 50 mg/kg (n = 8), IR (n = 9), or JIB-04 with IR (2 Gy, given 4 hr after drug administration; n = 8) for a total of 12 doses. Graph represents the tumor volume (left) and percent survival (right). DEF500 = (days to reach 500 mm^3 for JIB-04+IR-treated mice days to reach 500 mm^3 for JIB-04 treated mice)/(days to reach 500 mm^3 for IR-treated mice days to reach 500 mm^3 for vehicle-treated mice). Error bars represent SEM.

(B) Subcutaneous tumors generated from A549 cells treated as described in (A) with vehicle (n = 8), JIB-04 50 mg/kg (n = 8), IR (n = 9), or JIB-04 with IR (n = 10). Graph represents the tumor volume (left) and percent survival (right). DEF400 was calculated as above for time to 500 mm^3.

For (A) and (B), error bars represent SEM. ***$p < 0.001$ JIB-04+IR versus IR (2-way ANOVA for tumor growth in the left panel, and Kaplan-Meier for survival in the right panel).

(C and D) Tumor tissues were harvested at time of death (n = 4 for vehicle and JIB-04) or 12 hr after the last dose of treatment (n = 3 for IR and JIB-04+IR), tumor extracts were prepared, and H3K4me3 demethylase activity was measured. *$p < 0.05$ for IR versus no IR (C); *$p < 0.05$ for vehicle+IR/vehicle versus JIB-04+IR/JIB-04 alone (D) (t test).

See also Figure S8 and Table S3.

REAGENT or RESOURCE	SOURCE	IDENTIFIER
Antibodies		
Anti–phospho-Histone γH2AX (Ser139)	Millipore	Cat#05–636; RRID: AB_309864
Anti–tri-methyl-histone H3K9	Millipore	Cat#07-442; RRID: AB_310620
Anti-tri-methyl-histone H3K4	Millipore	Cat#07-473; RRID: AB_1977252
Anti-53BP1	Cell Signaling Technology	Cat#4937; RRID: AB_106954558
Anti-KDM5B	Cell Signaling Technology	Cat#3273; RRID: AB_1264191
Anti-KDM4B	Cell Signaling Technology	Cat#D7E6; RRID: AB_11140642
Anti-mouse IgG-HRP linked	Cell Signaling Technology	Cat#7076; RRID: AB_330924
Anti–Rad51	Abcam	Cat#ab-213; RRID: AB_302856
Anti-DNA-PKcs p-T2609	Abcam	Cat#ab-18356; RRID: AB_444447
Anti-H3	Abcam	Cat#ab-12079; RRID: AB_298834
Anti-HA (3F10)	Roche	Cat#11867423001; RRID: AB_10094468
Anti-Flag (M2)	Sigma-Aldrich	Cat#F1804; RRID: AB_262044
Anti-tubulin	Sigma-Aldrich	Cat#T5168; RRID: AB_477579
Anti-KDM5A	Bethyl	Cat#A300-897A: RRID: AB_2234038
Anti-KDM4A	Bethyl	Cat#A300-861A; RRID: AB_069461
Anti-KDM5C	Novus Biological	Cat#NB100-55328; RRID n/a
Anti-Ku70	Santa Cruz	Cat#sc-1487; RRID: AB_632614
Anti-goat IgG HRP conjugated	Santa Cruz	Cat#sc-2020; RRID: AB_631728
Anti-GAPDH	GeneTex	Cat#GTX100118; RRID: AB_1080976
Alexa Fluor 488–conjugated goat anti-Rabbit	Thermo Fisher	Cat#A-11034; RRID: AB_2576217
Alexa Fluor 555–conjugated goat anti-mouse	Thermo Fisher	Cat#A32727; RRID: AB_2633276
Rhodamine red–conjugated goat anti-mouse	Thermo Fisher	Cat#R-6393; RRID: AB_2556550
IRDye 680RD –conjugated goat anti-mouse	LI-COR Biosciences	Cat#925-68070; RRID: AB_2651128
IRDye 800 CW –conjugated goat anti-rabbit	LI-COR Biosciences	Cat#925-32211; RRID: AB_2651127
Chemicals, Peptides, and Recombinant Proteins		
JIB-04	Synthesized in-house (Wang et al., 2013)	N/A
GSK-J4	Tocris Bioscience	Cat#4594
GSK-J5	Tocris Bioscience	Cat#4689
PBIT	Sigma-Aldrich	Cat#PH009215
I-SceI enzyme	New England Bio Labs	Cat#R0694L
Critical Commercial Assays		
Ingenio Electroporation kit	Mirus Bio LLC	Cat#MIR 50115
H3K4me3 demethylation kit	Epigentek	Cat#P-3083
H3K9me3 demethylation kit	Epigentek	Cat#P-3081
EZ Magna ChIP A/G Chromatin Immunoprecipitation Kit	Millipore	Cat#17-100086
Experimental Models: Cell Lines		

REAGENT or RESOURCE	SOURCE	IDENTIFIER
U-2 OS	Dr. Sandeep Burma	N/A
LNCaP	Dr. Phil Thorpe	N/A
H1299	Dr. John D. Minna	N/A
A549	Dr. John D. Minna	N/A
HCC95	Dr. John D. Minna	N/A
HCC1195	Dr. John D. Minna	N/A
HCC2279	Dr. John D. Minna	N/A
HCC1719	Dr. John D. Minna	N/A
HBEC30KT	Dr. John D. Minna	N/A
HBEC3KT	Dr. John D. Minna	N/A
Experimental Models: Organisms/Strains		
Female athymic nude mice (nu/nu, 5–6 weeks old)	The Jackson Laboratory	Stock #: 002019
Oligonucleotides		
siRNA for Knock Down experiments	See Table S5	N/A
Oligonucleotides for RealTime Quantitative PCR	See Table S6	N/A
Recombinant DNA		
NHEJ-I reporter construct	Seluanov et al. (2010)	N/A
HR reporter construct	Seluanov et al. (2010)	N/A
Flag-KDM5B construct	Dr. Ralf Janknecht	N/A
HA-KDM5A construct	Addgene	plasmid #14799
HA-KDM4B construct	Addgene	plasmid #24181
HA-KDM4A construct	Dr. Yang Shi	N/A
Software and Algorithms		
ImageJ	NIH	https://imagej.nih.gov/ij/download.html
CellProfiler	Broad Institute	http://cellprofiler.org/releases/